

Needle Placement for Robot-Assisted 3D Ultrasound-Guided Breast Biopsy: A Preliminary Study

Sergio Jacobo-Zavaleta , Jorge Zavaleta 

Abstract—This work describes a new robot-assisted three-dimensional ultrasound-guided needle placement for breast biopsy to improve cancer diagnosis by automating needle trajectory, simplifying manual insertion and alleviating radiologist fatigue. In this way, basic robot requirements were first determined based on linking a free-hand ultrasound-guided breast biopsy with a whole-breast volumetric reconstruction system as part of a clinical workflow for breast cancer diagnosis. For modeling, a five-degree-of-freedom open-chain robot was proposed by considering the woman’s breast volume and a radial ultrasound scanning approach as workspace. The forward and inverse kinematics were calculated using the screw axis-based theory and a geometric-algebraic formulation, respectively. For trajectories, a collision-free path algorithm was computed to assess target reachability. For simulating, a dedicated biopsy environment was implemented in MATLAB-Simulink to perform multiple simulations by modifying some radiologist-manipulability variables in accordance with a factorial-method research design. The results showed a numerical and graphical verification of the equations and even a visual one of the needle placement during two stages: before a biopsy and after it. In conclusion, it was computationally explored the use of a novel robot-assisted needle placement in breast biopsy for women in a prone position.

Index Terms—Breast biopsy, Modeling, Needle placement, Robot-assisted, 3D ultrasound

I. INTRODUCTION

Breast cancer is the most diagnosed cancer in women around the world [1]. In 2020, the Global Cancer Statistics reported about 2.3 million new registered cases with an Age-standardized incidence of 47.8 per 100 000 people surpassing any other female cancer by representing 24.5% of all cancer types worldwide. In high and very high Human Development Index countries, the incidence rate reached higher values of up to 55.9 per 100 000 people, such as the alarming rate in Peruvian women of 35.9 [2]. Surprisingly, 15.5% of those women aged 30-59 underwent a breast clinical examination [3] and in 2021, nearly 70% of all cases of cancer were detected at late stages [4].

Clearly, early detection is the primary strategy for reducing mortality risk by promoting healthy lifestyles, prevention activities and the inclusion of noninvasive technology [5]. In that way, ultrasound (US)-guided breast biopsy is an accurate

minimal invasive procedure for tissue sampling under real-time and radiation-free imaging guidance to confirm the malignancy of a suspected lesion routinely visualized on US [6]. In addition to being a well-tolerated treatment (no painful breast compression), it’s relatively fast and widely available [7]. Current biopsy types generally include fine-needle (FN), core-needle (CN) and vacuum-assisted aspirations. Percutaneous biopsies are naturally operator dependent because they require skills, training and experience in US visualization and needle manipulability. Therefore, lacking these conditions lead to needle misplacements, repetitions, bleeding, patient discomfort and eventually, physician fatigue [8]. Such is the case of the free-hand or hand-held US-guided biopsy technique considered as a standard method at most hospital levels.

For these reasons, we describe a preliminary breast biopsy system to overcome the limitations discussed above by the combination of robot-assisted needle guidance with a three-dimensional (3D) Automated Breast Ultrasound System (ABUS) system for acquiring 3D volume data and localization of breast lesions in radial scanning. This solution was inspired by the advantages of current image-guided biopsies and a wide availability of US-based technology. Implying that needle paths shall not be as horizontal as possible due to accurate 3D visualization, leading to correct oblique insertions in contrast to two-dimensional (2D) US guidance. This proposal might increase the speed and accuracy of cancer diagnosis in women by reducing the false negative rate of breast biopsy and manual limitations of radiologists in clinical practice, especially in the hands of less experienced physicians.

The rest of the manuscript is organized as follows: Section II presents relevant works in robotic-assisted US-guided biopsy systems in the last two decades. Based on a possible integration of automated 3D US imaging into breast biopsy, Section III describes the requirements, restrictions and assumptions used to model, simulate and verify the expected clinical robot behavior. The results are described Section IV. Finally, we conclude the manuscript and point out the future directions of a partial validation before a real implementation.

II. RELATED WORKS

In the last two decades, experimental robotic US-guided biopsy systems have been designed to improve the current medical practice by combining the accuracy and maneuverability of robots to operate instruments with the safety and real-time capabilities of US imaging [9]. US-based technology stands out for managing 2D and 3D

Sergio Jacobo-Zavaleta is with Universidad Nacional de Trujillo, e-mail: sjacobo@unitru.edu.pe

Jorge Zavaleta is a Postdoctoral Research at at the State University of Rio de Janeiro (UERJ) in the project CAPES-Telemedecine and Medical Data Analysis, e-mail:zavaleta@pet-si.ufrj.br

image reconstruction after a whole-breast scanning and other advantages more in Table I. Particularly, 3D ABUS is a reliable tool for accurate localization of lesions and surroundings [10]. Some robotics challenges in breast biopsy include needle tracking [11], needle insertion under the shortest distance approach [12], autonomous needle insertion [13] and flexible needle steering [14]. Over the years, these systems have achieved needle position errors in the range 0.54-3.21 mm for targeting trajectories [9], [15].

In most cases, the basic procedure begins scanning the breast region to generate an image-based model to identify the biopsy target and select an insertion point. Then, before the radiologist completes the insertion by either manual or automated control, the robot orients the needle along a prescribed path [16]. The latter is generally accomplished with the help of a dedicated needle guide as end effector [15], [17]. However, these systems stand out for the lack of a practical and sequential integration of automated 3D US-image guidance into a breast biopsy performed in situ at the same time.

III. PROPOSED SOLUTION

A. Robot-Assisted Biopsy Workflow

Based on Table I, a 3D US-based robot-assisted biopsy workflow for women in a prone position was proposed to take advantage of automated US scanning in cancer diagnosis. As we can observe in Fig. 1, the workflow was divided into two main stages. The workspace’s elements are shown in Fig. 2.

The distal part of the robot known as the end effector operates as a pivot point for a safe and manual insertion of needles along a straight-line trajectory thanks to volumetric reconstructions of breast tissue and anatomical plane acquired by an ABUS system for target localization. However, the shared space between the breast volume and the robot under a biopsy table, led to the proposal an intermediate mechanism to connect both stages by using a breast holder device. This kind of container considers soft breast compression caused by woman weight to immobilize and stabilize tissue movements, resulting in a much more homogeneous US echo frequency pattern for scanning than in a supine position [19]. As a result, a restricted needle access is possible for an immediate biopsy.

B. Breast Modeling

Firstly, four different well-defined truncated cone models were calculated using anatomical metrics and breast-size profile equations reported by [20] as part of a breast volume characterization. Table II summarizes the data used for geometrical models (labeled as A, B, C and D according to bra cup sizes) of truncated conical surfaces defined by

$$zc = H_{holder} - \frac{H_{holder}(r - R_{lower})}{R_{upper} - R_{lower}} \quad (1)$$

where, zc is the relative height of a truncated cone given any conical radius r . Secondly, flexible breast models without internal structures were used to verify needle deformation. To do that, a Rayleigh damping method was implemented in Matlab-Simulink using reduced-order flexible solid model blocks. The stiffness values and mass matrices were computed as follows. First, finite-element (FE) meshes were generated from Computer Assisted Design (CAD) geometries and a Craig-Bampton order reduction. Second, the reduced model damping matrix was computed by setting a damping ratio of 0.215 [21]. Some breast models requirements [22], boundary conditions and material property values such as breast Young’s modulus ($E_{breast} = 0.9$ kPa [23]), breast skin density ($\rho_{breast} = 1\ 100$ kg/m³ [24]), breast skin Poisson ratio ($\eta_{breast} = 0.495$ [21]) and target density ($\rho_{lesion} = 1\ 170$ kg/m³ [25]) were also required to mesh a biomechanical breast model. A simulated lesion was mimicked by the inclusion of a stiff-region spherical volume of 3 mm radius. Even though intensive FE models were not covered in this work (the meshing element size was larger than suggested due to computational limitations), its implementation helped verify flexible needle behavior. Finally, four conical volume-based sets of points (for A, B, C and D sizes) were estimated as possible biopsy targets of 59 171, 80 197, 115 214 and 136 038 points.

TABLE I
CONVENTIONAL BREAST BIOPSY GUIDE SYSTEMS [18].

System	Advantages	Disadvantages
US ^a	Real-time imaging Radiation free Low-price technology	Irregular breast compression
Stereotactic ^b	Patient prone position Use of needle guides	High-price technology Painful breast compression
MRI ^c	Soft immobilization devices Use of needle guides Radiation free	High-price technology Limited space Electric/electronic limitations

^a: Ultrasound. ^b: Using Mammography. ^c: Magnetic Resonance Image.

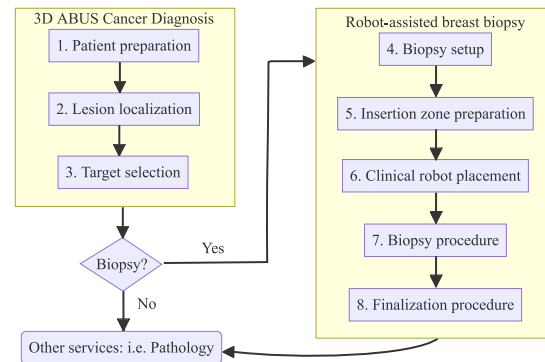


Fig. 1. Robot-assisted biopsy workflow.

TABLE II
DIMENSIONS OF TRUNCATED CONICAL BREAST MODELS

Cup ^a	Base radius R_{upper}	Top radius R_{lower}	Height H_{holder}
A	56.2	22.0	57.0
B	58.1	27.4	71.0
C	66.3	35.9	94.0
D	69.8	47.2	97.0

^a: Left and right breast size were considered very similar.

C. Breast Holder Device

The device was inspired by experimental MRI-based breast containers [26] and commercial MRI-based grid methods for breast immobilization [27]. The purpose of this proof design is to be a double-function mechanism for either US imaging (compact scanning structure) or biopsy (foldable device with limited needle access) as shown in Fig. 2. Therefore, the device tries to solve the US-coupling phenomenon through dry contact using photoacoustic materials such as polyethylene terephthalate glycol, polymethylmethacrylate, and polymethyl pentene [28]. Previous works suggest a wide range of material thickness (10-38 mm) [29], [30], including a gel stand-off pad (10-20 mm, Aquafex[®] gel). In this case, it was considered a thickness of 10 mm.

D. Robot Modeling

In contrast to medical robots that have 6 or 7 Degree-Of-Freedom (DOF), this robot was modeled as a dedicated 5-DOF open-chain mechanism as shown in Fig. 3. The absence of needle rotation around the insertion axis in the conventional biopsy procedure [31] was intentionally replicated for the end effector by removing 1-DOF. The sequence of robot articulations or joint types was defined as RPRPP (R, rotational; P, prismatic) of values θ_i . Not only this robot puts its end effector closer to the breast (by controlling joints 2, 3 and 4), but also it serves as a pivot point for a manual needle insertion along a straight-line direction (by displacement of joint 5). A whole-breast rotation ensures that any radial plane can be accessed (by rotation of joint 1). For security reasons, the last joint was kept as a non-motorized actuator, allowing the radiologist to control the invasive step as usual. According to the workflow, the robotic interaction was divided into two sequential stages called preplacement and postplacement focused on robot (before biopsy) and needle placement (after biopsy) respectively.

About the end effector, it was proposed a linear rail system (a pair of linear bearings and a pair of high-precision lead screws separated by the average palm width) to obtain an accurate, manual and stable motion of the biopsy needle, previously mounted on an interchangeable needle guide in link 5 (in yellow color). The prismatic-joint mechanism was inspired by an experimental US-guided breast biopsy robot in [17]. However, to verify this preliminary concept in a robot-assisted biopsy needle placement by considering physical constraints related to 3D US-image guiding in prone-position,

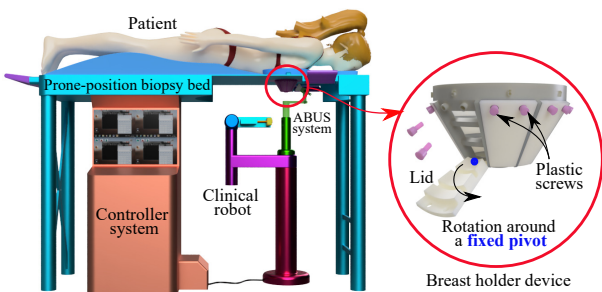


Fig. 2. Robot-assisted 3D US-guided breast biopsy workspace.

a geometrical approach based on only kinematic modeling of rigid bodies was initially enough to verify its theoretical feasibility in terms of reachability rates of different target positions. Therefore, external forces and torques caused by human-robot interactions were not considered.

1) *Robot Dimensions*: To calculate the values in Table III, two robot configurations in valid minimum ($\theta_2 = 0$) and maximum ($\theta_2 = \theta_{\max}$) poses by restricting insertion paths perpendicular to every holder's surface were examined, before comparing and defining a general model. In any case, the robot height was limited by the maximum height of a commercial biopsy table ($H_{\text{table}} = 1.1$ m) [32].

2) *Forward Kinematics*: For a modern way to describe rigid motions, an exponential coordinate representation was used. This geometric interpretation, like quaternions or Denavit-Hartenberg representation, has a powerful and alternative role in robotics [33]. Using the kinematic configuration of Fig. 3, the position and orientation of any reference frame or just frame attached to a robot joint denoted by $\{i\}$ was calculated by the product of exponentials formula as a homogeneous transformation matrix of 4×4 size. Thus, the end-effector configuration at $\{t\}$ is written as $\mathbf{T}_{st} = e^{[\mathcal{S}_1]\theta_1} \dots e^{[\mathcal{S}_{n-1}]\theta_{n-1}} e^{[\mathcal{S}_n]\theta_n} \mathbf{M}$. Where \mathbf{M} is the robot home position when $\mathbf{T}(\theta = 0)$ and \mathcal{S}_i is a screw axis (unified description of linear v and angular velocities ω as a normalized six-dimensional vector). This systematic description for kinematics has the advantage of eliminating the need of all joint frames and low-cost computing [34].

3) *Inverse Kinematics*: Due to the lack of a straightforward method for obtaining a convergent solution, a geometric-algebraic solution was used to generate a dedicated model. Given the end-effector position h_c and direction n_c from $\{c\}$, the robot joint positions were calculated as follows

$$\theta_1 = \begin{cases} q_1 + \pi & \text{If } q_1 = \text{atan2}(h_{sy}, h_{sx}) \geq 0, \\ q_1 - \pi & \text{Otherwise,} \end{cases} \quad (2)$$

$$\theta_3 = \text{atan2}(r_{33}, r_{13}), \quad (3)$$

$$\theta_4 = \frac{r_{14} + H_1 - L_3 \cos(\theta_3)}{\cos(\theta_3)}, \quad (4)$$

$$\theta_2 = r_{34} - L_2 - H_2 - \sin(\theta_3)(L_3 + \theta_4). \quad (5)$$

where, r_{14} and r_{34} are elements of a generic rotation matrix \mathbf{R}_{s1} from \mathbf{T}_{1t} calculated by matrices' decomposition as

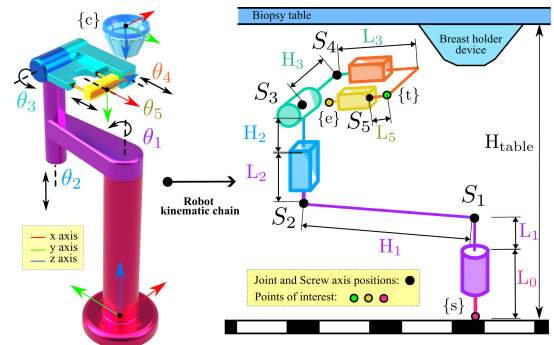


Fig. 3. Configuration for the 5-DOF open-chain clinical robot.

$$\mathbf{T}_{st} = \mathbf{T}_{s1} \mathbf{T}_{1t} \quad \text{if} \quad \mathbf{T}_{s1} = e^{[\mathcal{S}]\theta_1} \mathbf{M}_{01} \quad (6)$$

$$\mathbf{T}_{1t} = \mathbf{T}_{s1}^{-1} \mathbf{T}_{st} \quad (7)$$

E. Trajectory Generation

To visually verify robot kinematics, trajectories were generated in joint space for several reasons, including fast computing and ease of verifying joint limits and restrictions.

1) *For Preplacement*: Before end-effector placement in the right position, it was necessary to ensure a collision-free path between it and the desired target passing through the holder device using a non-image based collision-detection algorithm that works on the basis of assuming radial US images as biopsy planes [35] and the shortest insertion distance [36]. A priori, the holder device meant reducing radiologists' field of view in contrast to conventional biopsy, where needle manipulability is unrestricted so that horizontal insertions can be performed in accordance with biopsy guidelines [37]. Considering only a theoretical oblique insertion approach.

Regarding robot collisions, Fig. 4 shows three well-defined types primarily caused by the obstruction of the needle along its insertion direction (\mathbf{n}_c) to reach the target (\mathbf{p}_c). Whereas the first two types could be tested by needle-holder contact, the third one was checked by needle tip's proximity to the abdominal chest wall (D_{sep}) to avoid any unwanted puncture.

2) *Path Planning*: Given the starting and ending (\mathbf{h}_s) robot positions, the end-effector path was generated directly along a series of waypoints calculated using robot kinematics.

3) *Trajectory Planning*: It was proposed a coordinated trajectory (the first four joint movements finish at the same time) with a spline interpolation for getting smooth accelerations [33].

TABLE III
MAIN ROBOT DIMENSIONS AND JOINT LIMITS.

Dimension	Length (mm)	Joint	Range
L_0	625.00		
L_1^a	35.00		
H_1^a	300.00	θ_1	$[-\pi, \pi]$ rad
L_2	171.00	θ_2	$[0, 171]$ mm
H_2^a	45.00	θ_3	$[-\pi/2, \pi/2]$ rad
H_3^a	100.00	θ_4	$[0, 113]$ mm
L_3	222.00	θ_5	$[0, \theta_4 + 120^a]$ mm
L_5^a	5.47		

^a: Initially defined for CAD modeling.

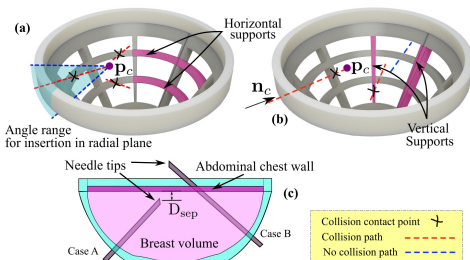


Fig. 4. Collision types for needle insertion algorithm. (a) Type 1, (b) type 2 and (c) type 3 collisions.

4) *For postplacement*: Here the end effector is pulled back to a suitable position $\theta_5 = -D_{EE \max}$ to mount the needle. Then, by pushing the device forward until at position $\theta_5 = -D_{EE \min}$, the needle tip is supposed to reach the target. Both distances are calculated by

$$D_{EE \min} = \begin{cases} L_{\text{needleFN}} - (\|\mathbf{tp}_s\| + L_5) \\ L_{\text{needleCN}} - (\|\mathbf{tp}_s\| + L_5) + \frac{L_{\text{throw}}}{2} - L_{\text{dead space}} \end{cases} \quad (8)$$

$$D_{EE \max} = \theta_4 + \text{Offset}_{L_5} - (L_5 + L_{\text{needleFN or needleCN}}) \quad (9)$$

where, L_{needleFN} y L_{needleCN} are needle lengths, $\|\mathbf{tp}_s\|$ is the distance from $\{t\}$ to needle tip, L_5 is the distance from $\{t\}$ to joint 5's position, L_{throw} and $L_{\text{dead space}}$ are specific dimensions of core needles and Offset_{L_5} is a constant length of link 3. In CN cases, it was taken into account a short distance away from the target to accommodate for the firing distance such that the sampling notch of the needle intersects the target [38].

F. Statistical Analysis

To measure the simulated effectiveness of the robot to align the needle pathway with the target to be sampled, the kinematic model and a free-collision needle path algorithm based on trajectory generation were tested in multiple controlled situations, where the supposed radiologist intervention was represented by the manipulation of two kinds of biopsy devices. To achieve this, a factorial-method design was proposed to assess the effects of two independent variables with varying values [39]. Given the variables of breast holder size and needle type, it required eight simulation groups (A-FN, A-CN, B-FN, B-CN, C-FN, C-CN, D-FN and D-CN). However, the minimum number of experiments for each group was initially unknown requiring a sampling method.

1) *Biopsy targets sampling*: Although the total population size of possible biopsy targets inside a woman's breast is infinite, a reasonable size (N) was estimated by thousands of vector positions (more than 59 000) for each breast volume. However, because of the high cost of computing all targets was not feasible, a double sampling was implemented to get a minimum set of randomized target positions to depict breast cancer cases and simulate the whole robot-assisted biopsy model. First, the free-collision needle path algorithm was run in Matlab for a medium-size sample ($n_1 = 1\,000$) to calculate its proportion-based parameter \hat{p}_1 (mean of reachable targets). Second, a small-size sample n_2 was estimated using the statistical theory of inference for population proportion [40]. Finally, after comparing the eight sample sizes and choosing the higher value for the same breast holder, it was obtained only four sample sizes (n_{2A} , n_{2B} , n_{2C} and n_{2D}) to cover all experiments. The randomized strategy was approached by the Latin Hypercube Sampling to get samples that reflect the true underlying distribution for computer experiments [41].

2) *Biopsy success rate*: To analyze the proficiency of this robotic system, it was defined a success rate based on the number of biopsy targets reached by the needle and if targeting errors (for position and direction) were lower than cut-off values. Therefore, this rate was calculated as the mean of cases in which both conditions were not met. The Euclidean position

error was measured from the target's centroid to needle tip position. The angle between the expected insertion path and final needle axis was calculated as direction error. A total of $2(n_{2A} + n_{2B} + n_{2C} + n_{2D})$ Simulink simulations were exported, plotted and analyzed using the statistical software Rstudio.

G. Simulation

1) *Robotic biopsy Procedure*: Before simulating, the robot interaction with workflow elements was defined in Fig. 5.

2) *Simulator setup*: Parameters are listed in Table IV. The robotic workspace and trajectory generation were implemented in MATLAB-Simulink as a based-design model under a supervisory control to manage the robot placement.

IV. RESULTS AND DISCUSSION

In spite of the absence of an experimental setup to validate the breast biopsy workflow, a total of nearly 1 000 simulations (Table V) were computed to verify the theoretical robot-assisted needle placement by the intersection of a needle tip (gray) with a target (red) as shown in Fig. 6.

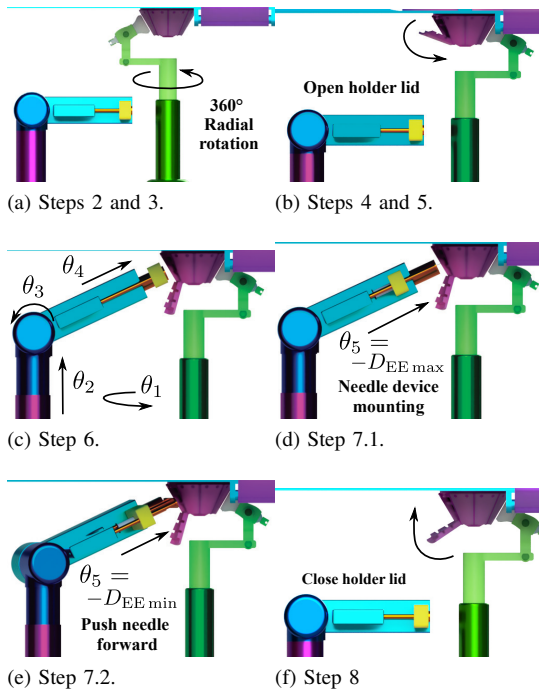


Fig. 5. Robot procedure according to the clinical workflow.

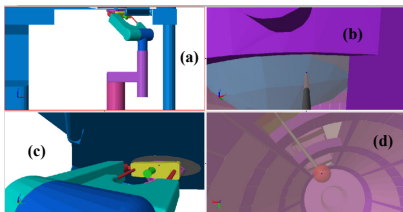


Fig. 6. Biopsy simulation during postplacement. (a) Lateral-side table, (b) FN needle, (c) radiologist and (d) target views.

A. Biopsy Success Rate

Fig. 7 shows that not all targets could be accessible due to robot model limitations or breast holder restrictions such as inevitable type 1 or 2 collisions. Furthermore, FN needles provided better chances of reaching the target than using CN ones, where the smaller the cup size, the lower the rate. The best performance related to D-cup holders reflects the importance of larger cups in minimizing most collision types.

Table VI shows that type-1 collisions (Col1) are needle independent and roughly less than one-third of them were inevitable (iCol1). Respecting type-2 collisions, the larger amount initially detected (pCol2) with CN needles was due to its bigger diameter. However, most type-2 collisions could be avoided by a small-angle rotation (around z_c) of the holder device, leading to a free-obstacle path in most cases. Finally, the danger of an unwanted puncture at the chest wall (Col3) was three times higher with CN needles, as expected.

Even though dynamic modeling was not considered, our geometric approach based on kinematic modeling led to assessing the impact of needle placement under physical constraints imposed by a new breast holder device. Modern techniques imply the inclusion of tissue-needle modeling, torsional friction modeling and obstacle avoidance by implementing actuator models and force-torque sensors in needle base [42].

B. Targeting Error

The mean values for targeting errors are summarized in Table VII. The similarity of errors using only CN needles explains the absence of significant and visible effects of breast cup size. On the contrary, there were slight errors in FN needle insertion paths. Certainly, lower diameters might have been affected by targets (a high-density region) during insertion.

TABLE IV
EXTRA SIMULATION SETTINGS.

Parameter	FN	CN
Offset _{prePlacement} ^a		5 mm
D _{sep}		1 mm
Needle gauge	20 G	14 G
Needle throw	-	10 mm
Needle dead space	-	8 mm
Needle lengths	50, 60, 80, 100, 120, 150 mm	

^a: Distance from $\{t\}$ to breast holder's outer surface.

TABLE V
GROUPED EXPERIMENTS FOR MULTIPLE SIMULATIONS.

Holder device	Biopsy needle FN	CN	Total
A	160 ^a	160 ^a	320
B	137 ^b	137 ^b	274
C	98 ^c	98 ^c	196
D	87 ^d	87 ^d	174
Total	482	482	964

^{a,b,c,d}: Samples of n_{2A} , n_{2B} , n_{2C} and n_{2D} size, respectively.

According to previous works, image-guided breast biopsy systems are usually evaluated as part of a diagnostic test, using metrics such as sensibility and specificity for sampled lesion diagnosis, which was not the case. Unfortunately, similar approaches for target reachability are not explicitly reported. Bluvolet *et al.* [38] reported a stereotactic-validated US needle guidance system for biopsy with a minimum success rate of up to 93% compared to 87% by the free-hand US technique. Suthakorn *et al.* [43] compared the influence of a needle holder in US-guided breast biopsy navigation. They confirmed that using a holder tool increases the success rate for inexperienced physicians (97.5%) when compared with only the free-hand method (57.5%). Being this last clearly surpassed by the robot performance. On top of that, position error values are inside the reported limits in experimental setups [9], [15].

Our study had several limitations. First, it was not considered internal and external phenomena that affect repetitive tasks and accuracy in real applications, such as material resistance, motor backlash and forces at the end effector. By performing these extra modeling in dynamic, electrical, stress and vibrational terms, a better realistic non-rigid model of the whole robot could have been obtained. Second, the proposal of a non-validated concept of a rigid breast holder device that could easily be part of another study.

V. CONCLUSIONS

This work introduced a clinical robot to assist the radiologist in performing a 3D US-guided breast biopsy for women in a prone position. The robot provides a needle guide for manual insertion by a linear movement of its end effector. The effectiveness of the robot was experimentally determined by a computational simulation of a factorial-method design based on robot kinematic modeling and a free-collision needle path algorithm because of the natural constraints of using a new breast holder device for either automated radial US scanning or percutaneous biopsy. The results look promising due to robot-assisted biopsy success rate is higher than achieved on conventional US-guided biopsy, and targeting errors are compatible with other needle-guidance systems. This preliminary study might help solve the problem to automate and accelerate biopsy planning for treatments in clinics and hospitals that primarily rely on US-based technology by reducing the strong need of human control at low cost. Particularly, the accurate but not yet clinically standardized 3D ABUS systems for precise localization of lesions. Future works will focus on redesigning and validating the holder device model in terms of size, material and fabrication process to obtain a hands-on but US-friendly prototype.

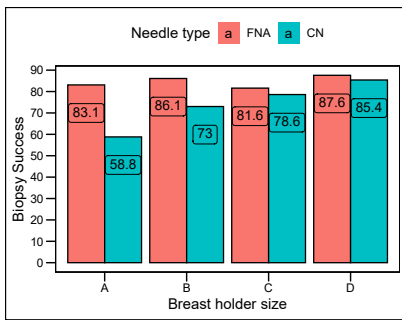


Fig. 7. Distribution of robot-assisted biopsy success.

TABLE VI
COLLISION RATES (%) FOR SIMULATED BIOPSIES.

Cup	Needle	Col1 ^a	iCol1 ^b	pCol2 ^c	Col2 ^d	Col3 ^e
A	FN	32.5	13.8	11.2	1.9	6.9
	CN	32.5	13.8	19.4	1.9	35.6
B	FN	30.7	10.2	9.5	1.5	5.1
	CN	30.7	10.2	16.1	1.5	22.6
C	FN	32.7	11.2	7.1	3.1	4.1
	CN	32.7	11.2	12.2	3.1	14.3
D	FN	27.0	6.7	11.2	1.1	3.4
	CN	27.0	6.7	12.4	1.1	10.1

a,b,c,d,e: Type-1, inevitable type-1, initial type-2, final type-2 and type-3 collisions, respectively.

TABLE VII
TARGETING ERRORS.

Cup	Needle	Mean errors at postplacement stage Position (mm)	Direction (°)
A	FN	1.06	0.57
	CN	2.97	4.58
B	FN	1.08	0.57
	CN	2.97	4.58
C	FN	1.22	1.15
	CN	2.97	0.57
D	FN	1.17	1.15
	CN	2.97	0.57

REFERENCES

- [1] N. Azamjah, Y. Soltan-Zadeh, and F. Zayeri, "Global Trend of Breast Cancer Mortality Rate: A 25-date Study," *Asian Pacific Journal of Cancer Prevention*, vol. 20, no. 7, pp. 43-46, 2019.
- [2] H. Sung, J. Ferlay, R. L. Siegel, M. Laversanne, I. Soerjomataram, A. Jemal, and F. Bray, "Global Cancer Statistics 2020: GLOBOCAN Estimates of Incidence and Mortality Worldwide for 36 Cancers in 185 Countries," *CA: A Cancer Journal for Clinicians*, vol. 71, pp. 209-249, May 2021.
- [3] Instituto Nacional de Estadística e Informática, "Peru: Enfermedades No Transmisibles y Transmisibles," tech. rep., Ministerio de Salud, 2020.
- [4] Centro Nacional de Epidemiología, Prevención y Control de Enfermedades, "Boletín epidemiológico del Perú, 2021," Tech. Rep. 05, Ministerio de Salud, Perú, Jan. 2021.
- [5] A. Adam, R. F. Dondelinger, and P. R. Mueller, "Interventional Radiology in Breast Cancer," in *Interventional Radiology in Cancer*, vol. 10.1007/978-3-642-18668-4 of *Medical Radiology*, p. 282, Springer-Verlag, first ed., 2004.
- [6] L. F. Smith, I. T. Rubio, R. Henry-Tillman, S. Korourian, and V. Klimberg, "Intraoperative ultrasound-guided breast biopsy," *The American Journal of Surgery*, vol. 180, pp. 419-423, Dec. 2000.
- [7] M. Raghu and R. Hooley, "Breast Ultrasound for the Interventionalist," *Techniques in Vascular and Interventional Radiology*, vol. 17, pp. 16-22, Mar. 2014.
- [8] H. Zhao, T. Liu, M. Chen, Q. Tian, Z. Li, S. Cao, and C. Ai, "A needle insertion concept and robot system for breast tumor," in *IEEE 2016 International Conference on Mechatronics and Automation - Harbin, Heilongjiang, China*, pp. 896-901, 2016.

- [9] M. Z. Mahmoud, M. Aslam, M. Alsaadi, M. A. Fagiri, and B. Alonazi, "Evolution of Robot-assisted ultrasound-guided breast biopsy systems," *Journal of Radiation Research and Applied Sciences*, vol. 11, no. 1, pp. 89–97, 2017.
- [10] J. C. M. van Zelst and R. M. Mann, "Automated Three-dimensional Breast US for Screening: Technique, Artifacts, and Lesion Characterization," *Radiographics*, p. 170162, 2018.
- [11] M. Chen, H. Zhao, Z. Li, Y. Zhao, Q. Tian, and T. Liu, "Development of a new needle insertion medical robot for breast tumor surgery," in *IEEE 2017 International Conference on Real-time Computing and Robotics (RCAR)*, Okinawa, Japón, pp. 28–33, 2017.
- [12] N. Tanaiutchawoot, B. Treepong, C. Wiratkapan, and J. Suthakorn, "A path generation algorithm for biopsy needle insertion in a robotic breast biopsy navigation system," in *IEEE International Conference on Robotics and Biomimetics (ROBIO) - Bali, Indonesia*, pp. 398–403, 2014.
- [13] S. O. Orhan, M. C. Yildirim, and O. Bebek, "Design and modeling of a parallel robot for ultrasound guided percutaneous needle interventions," in *41st Annual Conference of the IEEE Industrial Electronics Society IECON - Yokohama, Japón*, pp. 1–12, 2015.
- [14] M. Abayazid, P. Moreira, N. Shahriari, A. Zompas, and S. Misra, "Three-Dimensional Needle Steering Using Automated Breast Volume Scanner (ABVS)," *Journal of Medical Robotics Research*, vol. 1, no. 1, pp. 1–9, 2016.
- [15] M. K. Welleweerd, F. J. Siepel, V. Groenhuis, J. Veltman, and S. Stramigioli, "Design of an end-effector for robot-assisted ultrasound-guided breast biopsies," *International Journal of Computer Assisted Radiology and Surgery*, vol. 15, pp. 681–690, 2020.
- [16] A. Priester, S. Natarajan, and M. Culjat, "Robotic ultrasound systems in medicine," *IEEE Transactions on Ultrasonics, Ferroelectrics and Frequency Control*, vol. 60, pp. 507–523, Mar. 2013.
- [17] G. Megali, O. Tonet, C. Stefanini, M. Boccadoro, V. Paspasypoulos, L. Angelini, and P. Dario, "A computer-assisted robotic ultrasound-guided biopsy system for video-assisted surgery," in *International Conference on Medical Image Computing and Computer-Assisted Intervention - MICCAI (W. Niessen and M. Viergever, eds.)*, vol. 2208, pp. 343–350, Springer-Verlag, 2001.
- [18] L. Bartella, C. S. Smith, D. D. Dershaw, and L. Liberman, "Imaging Breast Cancer," *Radiologic Clinics of North America*, vol. 45, no. 1, pp. 45–67, 2007.
- [19] A. Farrokh, H. Erdönmez, F. Schäfer, and N. Maass, "SOFIA: A Novel Automated Breast Ultrasound System Used on Patients in the Prone Position: A Pilot Study on Lesion Detection in Comparison to Handheld Grayscale Ultrasound," *Geburtshilfe und Frauenheilkunde*, vol. 78, no. 5, pp. 499–505, 2018.
- [20] S. Y. Huang, J. M. Boone, K. Yang, N. J. Packard, S. E. McKenney, N. D. Prionas, K. K. Lindfors, and M. J. Yaffe, "The characterization of breast anatomical metrics using dedicated breast CT," *Medical Physics*, vol. 38, no. 4, pp. 2180–2191, 2011.
- [21] L.-H. Chen, S.-P. Ng, W. Yu, J. Zhou, and K. W. Frances Wan, "A study of breast motion using non-linear dynamic fe analysis," *Ergonomics*, vol. 56, no. 5, pp. 868–878, 2013. PMID: 23514244.
- [22] S. N. Bhatti and M. Sridhar-Keralapura, "A novel breast software phantom for biomechanical modeling of elastography: A novel breast software phantom for elastography biomechanics," *Medical Physics*, vol. 39, pp. 1748–1768, Mar. 2012.
- [23] J. Cheng, K. Brandt, R. Grimm, K. Glaser, and J. Kugel, "Noncompressive MR Elastography of Breasts," in *Proceedings of the International Society for Magnetic Resonance in Medicine*, (Salt Lake City, USA), p. 25, 2013.
- [24] ICRP, *Adult Reference Computational Phantoms*, vol. 39 of ICRP Publication 110. SAGE Publications, first ed., 2009.
- [25] T. Ohno, R. W. Sweet, D. Dejak, and S. Spiegelman, "Purification and characterization of the DNA polymerase of human breast cancer particles," *Proceedings of the National Academy of Sciences*, vol. 74, pp. 764–768, Feb. 1977.
- [26] W. Liu, Z. Yang, S. Jiang, D. Feng, and D. Zhang, "Design and implementation of a new cable-driven robot for MRI-guided breast biopsy," *The International Journal of Medical Robotics and Computer Assisted Surgery*, vol. 16, Apr. 2019.
- [27] Noras MRI products, "Breast Biopsy 7-Channel Coil BI 7 for Immobilization and MR-supported Mammography," tech. rep., NORAS MRI products, 2020.
- [28] M. Pramanik, G. Ku, C. Li, and L. V. Wang, "Design and evaluation of a novel breast cancer detection system combining both thermoacoustic (TA) and photoacoustic (PA) tomography," *Medical Physics*, vol. 35, no. 6, p. 2218, 2008.
- [29] S. Manohar and M. Dantuma, "Current and Future Trends in Photoacoustic Breast Imaging," *Photoacoustics*, vol. 16, p. 26, 2019.
- [30] A. Nikolaev, H. H. Hansen, L. De Jong, R. Mann, E. Tagliabue, B. Maris, V. Groenhuis, F. Siepel, M. Caballo, I. Sechopoulos, and C. L. De Korte, "Ultrasound-guided breast biopsy of ultrasound occult lesions using multimodality image co-registration and tissue displacement tracking," in *Medical Imaging 2019*, vol. 10955 of *Progress in Biomedical Optics and Imaging - Proceedings of SPIE*, pp. 1–8, SPIE, 2019.
- [31] R. D. Rocha, R. R. Pinto, D. P. B. A. Tavares, and C. S. A. Gonçalves, "Step-by-step of ultrasound-guided core-needle biopsy of the breast: Review and technique," *Radiologia Brasileira*, vol. 46, no. 4, pp. 234–241, 2013.
- [32] Hologic Inc., "The Affirm® Prone Biopsy System." [Online]. Available at <https://www.affirmpronebiopsy.com>, 2022. (accessed 05 June 2022).
- [33] K. M. Lynch and F. C. Park, *Modern Robotics: Mechanics, Planning, and Control*. Cambridge, UK: Cambridge University Press, 2017.
- [34] F. C. Park, "Computational aspects of the product-of-exponentials formula for robot kinematics," *IEEE Transactions on Automatic Control*, vol. 39, pp. 643–647, Mar. 1994.
- [35] A. Dominique, "Automatic Breast Ultrasound Scanning," in *Lobar Approach to Breast Ultrasound*, ch. 26, pp. 325–336, Springer-Verlag, first ed., 2018.
- [36] L. Apestegeua and L. J. Pina, "Ultrasound-guided core-needle biopsy of breast lesions," *Insights into Imaging*, vol. 2, no. 4, pp. 493–500, 2011.
- [37] K. S. Mahesh, "Screening for Breast Cancer," in *Breast Cancer Screening and Diagnosis: A Synopsis*, vol. 23, pp. 23–36, Springer-Verlag, first ed., 2015.
- [38] N. Bluvol, A. Shaikh, A. Kornecki, D. Del Rey Fernandez, D. Downey, and A. Fenster, "A needle guidance system for biopsy and therapy using two-dimensional ultrasound: A needle guidance system for biopsy and therapy," *Medical Physics*, vol. 35, pp. 617–628, Jan. 2008.
- [39] W. G. Zikmund, B. J. Babin, J. C. Carr, and M. Griffin, *Business Research Methods, 8th Edition*. South-Western College Pub, eighth ed., 2009.
- [40] A. C. Tamhane and D. D. Dunlop, *Statistics and Data Analysis : From Elementary to Intermediate*. Prentice Hall, 2000.
- [41] M. D. Mckay, R. J. Beckman, and W. J. Conover, "A Comparison of Three Methods for Selecting Values of Input Variables in the Analysis of Output From a Computer Code," *Technometrics*, vol. 42, pp. 55–61, Feb. 2000.
- [42] K. B. Reed, A. M. Okamura, and N. J. Cowan, "Modeling and control of needles with torsional friction," *IEEE transactions on bio-medical engineering*, vol. 56, no. 12, pp. 2905–2916, 2009.
- [43] J. Suthakorn, N. Tanaiutchawoot, C. Wiratkapan, and S. Ongwattanakul, "Breast biopsy navigation system with an assisted needle holder tool and 2D graphical user interface," *European Journal of Radiology Open*, vol. 5, pp. 93–101, 2018.



Sergio Augusto Jacobo Zavaleta, received his bachelor's degree in Mechatronics Engineering (2019) from the Universidad Nacional de Trujillo, Peru. His research interests include design of clinical robots and biomedical applications based on Artificial Intelligence using Machine Learning.



Jorge Juan Zavaleta Gavidia, received the Ph. D in Systems and Computer Engineering in the Federal University of Rio de Janeiro (UFRJ) in 2017. He received the title of master's in computer science from the Federal University of Rio Grande do Sul (UFRGS) in 1997. He received the title of Licenciante in Mathematics from the Universidad Nacional de Trujillo (UNT) in 1998 and received a bachelor's degree in Physical and Mathematical Sciences from the UNT in 1992. Professor of Computing and currently a researcher of postdoctoral at the State University of Rio de Janeiro (UERJ) in the project CAPES-Telemedicine and Medical Data Analysis. He is interested in topics research related to Data Science, Artificial Intelligence and Machine Learning.